

Eigenvalues of QCD Dirac matrix with improved staggered quarks in the continuum limit

Olaf Kaczmarek,¹ Ravi Shanker,^{2,*} and Sayantan Sharma²

¹*Fakultät für Physik, Universität Bielefeld, D-33615 Bielefeld, Germany*

²*The Institute of Mathematical Sciences, a CI of Homi Bhabha National Institute, Chennai, 600113, India*

We calculate the eigenmodes of the Highly Improved Staggered Quark (HISQ) matrix near the chiral crossover transition in QCD with $2 + 1$ flavors with the aim to gain more insights into its temperature dependence. On performing the continuum extrapolation, we do not observe any gap opening up in the infrared part of the eigenvalue density of QCD Dirac operator, instead we observe a peak. The existence of the peak and oscillations of the infrared eigenmodes can be understood in terms of an interacting ensemble of instantons. From the properties of the continuum extrapolated eigen spectrum we further show that the anomalous $U_A(1)$ part of the chiral symmetry is not effectively restored simultaneously along with its non-singlet counterpart. We provide an explanation for this observation, further showing interesting connections between the anomalous $U_A(1)$ restoration and the change in the infrared part of the eigenvalue distribution.

PACS numbers: 12.38.Gc, 11.15.Ha, 11.30.Rd, 11.15.Kc

Introduction The eigenvalue spectrum of the quark Dirac operator contains valuable information about the fundamental properties of Quantum Chromodynamics (QCD). The chiral condensate which acts as a (pseudo) order parameter for the chiral (crossover) transition in QCD is related to the density of near-zero eigenvalues [1]. In fact it was shown from very general considerations that the formation of the chiral condensate is related to the occurrence of small eigenvalues that scale proportional to the volume [2]. The breaking of the non-singlet part of chiral symmetry i.e. $SU_A(2) \times SU_V(2) \rightarrow SU_V(2)$ of QCD with physical quark masses at the crossover temperature $T_c = 156.5 \pm 1.5$ MeV [3] can also be explained in terms of modifications in the deep infrared part of the eigenvalue density. The flavor-singlet $U_A(1)$ part of the chiral symmetry on the other hand, is anomalous yet is believed to play an important role in determining the nature of the chiral phase transition [4–6]. The temperature dependence of the amount of $U_A(1)$ breaking near the chiral crossover transition in QCD can be only determined using non-perturbative lattice techniques and is a topic of contemporary interest in lattice QCD see for e.g. Ref. [7, 8] for recent reviews. Whereas there are some very compelling evidence that show $U_A(1)$ remains effectively broken in $2 + 1$ flavor QCD with physical quark mass m [9–15], even when $m \rightarrow 0$ [16], there are lattice studies which also favor an effective restoration at T_c [17–22].

The eigenvalue spectrum of the QCD Dirac matrix also encodes within it some remarkable universal properties. It was shown that the route towards achieving thermodynamic limit for the infrared modes of the Dirac operator is universal [23], for any number of light quark flavors. The existence of a non-zero chiral condensate leads to a sum rule involving sum of inverse squares of

these small eigenvalues [2]. These sum rules are universal irrespective of the details of the nature and type of gauge interactions [23, 24] and could be derived from chiral random matrix theory [25]. A good agreement was demonstrated for the distribution of the small eigenvalues and the spectral density of lattice QCD Dirac operator and chiral random matrix theory at zero temperature on small lattice volumes [26]. In fact universal correlations between higher order spectral functions in a random matrix theory has been derived [27] and its connection to QCD was discussed. At finite temperature the universal features of infrared eigenvalues can be also accounted for within a random matrix theory [28–30]. Additionally the infrared eigenvalue spectrum of QCD has more subtle features. A near-zero peak of localized eigenvalues has been observed for finite lattices, mixing with but very different from the delocalized bulk modes whose spectral density follows random matrix statistics [7, 31]. Whether or not such a feature survives in the continuum limit is yet to be ascertained. Previous studies of quark Dirac spectrum in an instanton liquid ensemble [29, 32] at zero temperature have observed similar peak-like feature.

With increasing temperature the localized modes starts separating out from the random bulk modes leading to the opening up of a mobility edge [31]. The corresponding temperature where a finite mobility edge separates the bulk modes from the localized one was initially estimated from lattice studies to be identical to T_c in dynamical [33–38] as well as in quenched QCD [39], reminiscent of an Anderson-like transition that is observed in disordered semi-metals [40]. However independent lattice studies do discuss another possible scenario where the opening of a finite mobility edge may occur at temperatures higher than T_c [41], with an intermediate phase consisting of scale-invariant infinitely extended infrared modes [42, 43] strongly interacting with the bulk modes leading to a singularity at the mobility edge.

Most of the previous lattice QCD studies were either performed in the quenched limit or with dynamical

*Electronic address: rshanker@imsc.res.in

ical quarks but away from the physical point and for finite lattice spacings. On a finite lattice, the most often used lattice discretization i.e. the staggered fermions only has a remnant of the continuum chiral symmetry group due to mixing of spin and flavor degrees of freedom. Furthermore the anomalous part of the chiral symmetry in the continuum is not realized exactly by the staggered/Wilson quarks and is expected to be recovered only in the continuum limit. We, for the first time study the properties of the eigenvalue spectrum of (highly) improved dynamical staggered Dirac operator in large volume lattices by carefully performing a continuum extrapolation. We show that the deep infrared spectrum of QCD Dirac operator has indeed a peak of near-zero modes which survives in continuum. These are distinct from other infrared modes which has a linearly rising density and a quadratic level repulsion similar to a certain class of random matrix theories. These so-called bulk modes are delocalized in volume as compared to the near-zero modes and they tend to distinctly disentangle from each other at a temperature $\sim 1.15 T_c$, which is also where $U_A(1)$ is *effectively* restored. In the subsequent sections we discuss our results and also provide a unified physical explanation of these phenomena we observe.

Numerical Details In this work we use the gauge configurations for 2 + 1 flavor QCD with physical quark masses generated by the HotQCD collaboration using Highly Improved Staggered quark (HISQ) discretization for the fermions and tree-level Symanzik improved gauge action. These ensembles have been previously used to measure the equation of state of QCD both at zero and finite baryon density [3, 44]. The Goldstone pion mass is set to 140 MeV and the kaon mass is 435 MeV for these configurations. We focus on five different temperatures, one below T_c and others above T_c . For most of these temperatures we consider three different lattice spacings corresponding to $N_\tau = 8, 12, 16$, details of which are mentioned in Table I in Appendix A. The number of spatial lattice sites was chosen to be $N_s = 4N_\tau$ such that the spatial volume in each case was about 4 fm, which ensures that the system is close to the thermodynamic limit. We next measure the eigenvalues of the massless HISQ Dirac matrix on these gauge ensembles using conjugate gradient method based algorithms.

General features of the eigenvalue spectrum of QCD using HISQ Dirac operator in continuum limit In this section we study in detail the eigenvalue density $\rho(\lambda)$ of the fermions in 2 + 1 flavor QCD by performing a continuum extrapolation of the parameters characterizing the eigenspectrum calculated on the lattice with Highly Improved Staggered Quarks (HISQ) discretization. We first study the eigenvalue spectrum for four different temperatures above T_c in order to understand whether the flavor singlet and non-singlet parts of the chiral symmetry is *effectively* and simultaneously restored or not.

At zero temperature it is known from chiral perturba-

tion theory [45] that the bulk eigenvalue density is

$$\rho(\lambda) = \frac{\langle 0|\bar{\psi}\psi|0\rangle}{\pi} + |\lambda|\langle 0|\bar{\psi}\psi|0\rangle^2 \frac{N_f^2 - 4}{32\pi^2 N_f F_\pi^4} + \dots \quad (1)$$

The intercept of the eigenvalue density gives the chiral condensate. The ratio of the slope and the intercept of the density as a function of λ should be proportional to the chiral condensate. We first focus on the intercept and the slope (linear in λ) of the eigenvalue density at the lowest temperature $T = 145$ MeV, shown in the left panel of Fig. 1, and compare with the expectations from Eq. 1. At this temperature we could only obtain a continuum estimate of the slope and intercept as we have data for two lattice spacings. From the continuum estimate of the intercept we obtain a chiral condensate $\langle 0|\bar{\psi}\psi|0\rangle/T^3 = 18.4$. From the slope we could similarly extract its square and hence the chiral condensate (normalized by T^3) to be 17.3 which is consistent with the one extracted from the intercept. Thus leading features of the eigenvalue density of QCD at 145 MeV are indeed very well represented within chiral perturbation theory.

The bulk eigenvalue density in the chirally symmetric phase has been studied very recently [46]. Most generally, it can be expressed as a function of λ as

$$\frac{\rho(\lambda)}{T^3} = \frac{\rho_0}{T^3} + \frac{\lambda}{T} \cdot \frac{c_1(T, m)}{T^2} + \frac{\lambda^2}{T^2} \cdot \frac{c_2(T, m)}{T} + \frac{\lambda^3}{T^3} c_3(T, m). \quad (2)$$

Here c_1 is the coefficient that characterizes the leading-order growth of the eigenvalue spectrum in the deep infrared and c_2 is its next-to leading order coefficient which eventually has a λ^3 -dependence predicted from perturbation theory. The intercept ρ_0 gives the the chiral condensate. The coefficients $c_{1,2,3}$ can in general be a function of the temperature T and the light-quark mass m .

The results of the eigenvalue density $\rho(\lambda)/T^3$ as a function of λ for $T > T_c$ are shown in the middle and right panel of Fig. 1. On the finest available $N_\tau = 16$ lattice, we observe two distinct features in the eigenvalue spectrum, a peak of near-zero eigenvalues and the linearly rising part, which we call as bulk modes. For $T \lesssim T_c$, the near-zero and the bulk eigenvalues overlap strongly making it impossible to distinguish them apart. At higher temperatures, the bulk eigenvalues separate out from the deep-infrared part of the spectrum allowing for near-zero modes to be distinctly visible. Comparing the results of different lattice spacings, we observe the same trend at each temperature above T_c i.e. near-zero peak gets smeared with the bulk for coarser lattices and becomes more prominent in the continuum limit. This is thus a physical feature of the eigen spectrum and not a lattice artifact. In order to interpret its origin we recall that in the instanton liquid model (ILM) at zero temperature, the scaled eigenvalue ($c\lambda$) density of the Dirac operator for N_f flavors and zero topological charge sector is distributed according to [47],

$$\rho(c\lambda) = \frac{c\lambda}{2} \left[J_{N_f}^2(c\lambda) - J_{N_f+1}(c\lambda)J_{N_f-1}(c\lambda) \right]. \quad (3)$$

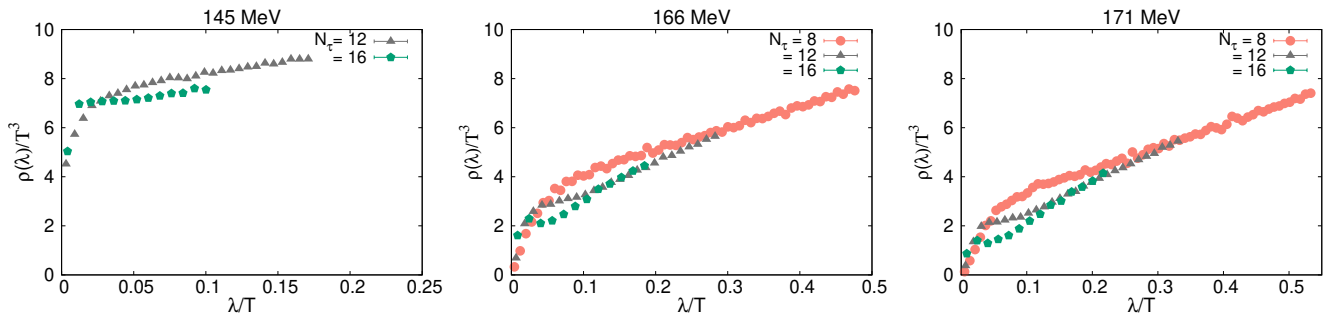


Fig. 1: Eigenvalue spectrum for HISQ Dirac operator for 3 different lattice spacings corresponding to $N_\tau = 8, 12, 16$ at $T = 166, 171$ MeV (center, right) and for two different lattice spacings, $N_\tau = 12, 16$ respectively at $T = 145$ MeV (left).

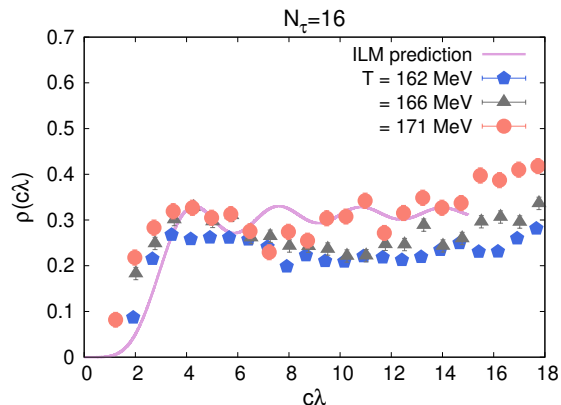


Fig. 2: Near-zero (scaled) eigenvalue density for HISQ Dirac operator at $T = 162, 166, 171$ MeV for the finest lattice spacing corresponding to $N_\tau = 16$ and its comparison with ILM prediction available at $T = 0$.

To compare our data with the above formula, we take $c = V\langle 0|\bar{\psi}\psi|0\rangle/T$, where V is the spatial volume of the system and $N_f = 3$. A comparison of near zero modes for three different temperatures, $T = 162, 166, 171$ MeV, is shown in Fig. 2 by removing the contribution of the bulk intercept ρ_0 . We observe a good agreement with ILM for $T = 171$ MeV, in particular, the initial few oscillations of the small eigenvalue density as a function of $c\lambda$.

Now focusing on the bulk modes, it was shown using chiral Ward identities that in the symmetry restored phase, the sufficient condition for $U_A(1)$ restoration evident from the degeneracy of up to 6-point correlation functions in the scalar-pseudo-scalar sector are $c_1 = \mathcal{O}(m^2) + \dots$ and $c_3 = c_{30} + \mathcal{O}(m^2) + \dots$. The perturbative λ^3 -growth in Eq. 2 can have a mass-independent coefficient which however does not lead to $U_A(1)$ breaking. We verify whether indeed it is true even non-perturbatively by performing a fit to the bulk part i.e. all eigenvalues $\lambda > \lambda_0$ with $\frac{\rho(\lambda)}{T^3} = \frac{\lambda}{T} \cdot \frac{c_1(T, m)}{T^2} + \frac{\rho_0}{T^3}$. This ansatz neglects higher powers in λ which is well justified since we are in the deep infrared of the eigen spectrum, represented by $\mathcal{O}(100)$ eigenvalues out of a total million available on

such lattice sizes. The results of the fit are discussed in Table II. The extracted slope c_1 for each temperature $T > T_c$, at three different values of N_τ then allows us to perform a continuum ($\sim 1/N_\tau^2$) extrapolation of this coefficient. We next study the m -dependence of this continuum extrapolated coefficient $c_1(m, T)$. The results of the fits are shown in Fig. 3. It is evident from the fit that it is more favorable that c_1 is proportional to T^2 ($\chi^2/\text{d.o.f.}=0.6$) to leading order rather than c_1 is proportional to m^2 ($\chi^2/\text{d.o.f.}=0.1$). From the fit we obtain the value of $c_1(m, T)/T^2 = 16.8(4)$.

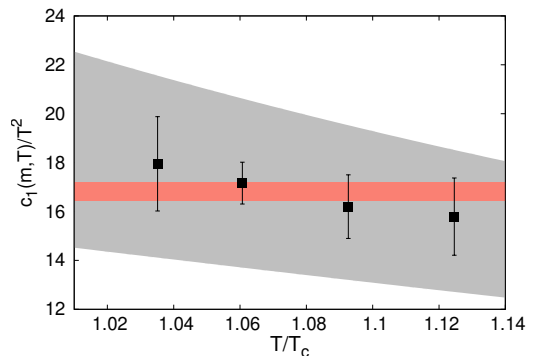


Fig. 3: Continuum estimates for $c_1(m, T)/T^2$ for $T > T_c$ obtained after fitting the points with a m -independent constant (orange band) and a sum of quadratic (m^2/T^2) and quartic (m^4/T^4) dependence (gray band).

This result for the slope in the continuum limit has a very important consequence, i.e. the m -independent term in c_1 ensures that the $U_A(1)$ part of the chiral symmetry will remain *effectively* broken in the chiral limit in the symmetry-restored phase. The coefficient of linear-in- λ term at finite temperature is significantly larger than its zero temperature value of 0.63 in units of T_c^2 obtained from Eq. 1. For extracting the later we have used the latest data for the chiral condensate and F_π from the FLAG review [48], for $N_f = 3$. A significant thermal enhancement in the slope of the eigen spectrum is observed above T_c . Moreover the slope of the eigen density for $T \lesssim 1.12 T_c$ is distinctly different from the perturbative

λ^3 rise implying significant non-perturbative effects.

The fate of $U_A(1)$ breaking in the continuum limit Since the flavor singlet part of the chiral symmetry is anomalous it has no corresponding order parameter. Hence to measure whether this singlet part of the chiral symmetry is simultaneously (and effectively) restored along with the non-singlet part, it has been suggested [49] to look at the degeneracies of the integrated correlators of mesons i.e., $\chi_\pi - \chi_\delta$. In the continuum, the integrated meson correlators are related to each others through the following relations, $\chi_\delta = \chi_\sigma - 4\chi_{\text{disc}}$ and $\chi_\pi = \chi_\eta + 4\chi_{5\text{disc}}$. These integrated meson correlators are defined as $\chi_\pi = \int d^4x \langle \pi^i(x)\pi^i(0) \rangle$, $\chi_\sigma = \int d^4x \langle \sigma(x)\sigma(0) \rangle$, $\chi_\delta = \int d^4x \langle \delta^i(x)\delta^i(0) \rangle$ and $\chi_\eta = \int d^4x \langle \eta(x)\eta(0) \rangle$ where $i = 1, 2, 3$. We measure $(\chi_\pi - \chi_\delta)/T^2$ at the four different temperatures above T_c , and perform a $\sim 1/N_\tau^2$ continuum extrapolation at each temperature, results of which are shown in Fig. 4. For the highest temperature we have only two data points available corresponding to $N_\tau = 8, 12$ for continuum extrapolation hence assigned a 40% and 20% error in slope and the intercept obtained from the fit, similar to that obtained for the previous temperature. It is evident that the continuum extrapolated values of this integrated correlator drops to 1/6 when T/T_c changes from 1.04-1.12 and a naive linear extrapolation of the intercept gives a temperature around $1.14 T_c$ when this observable goes to zero. In fact the values of this observable increase when the lattice spacings are made finer. Performing continuum estimates with finer lattice sizes $N_\tau = 16, 12$ at each temperature, gives a higher intercept than the corresponding extrapolation considering all three N_τ -values. Hence the finiteness of this observable is quite robust and we conclude that $U_A(1)$ does not get *effectively* restored at T_c .

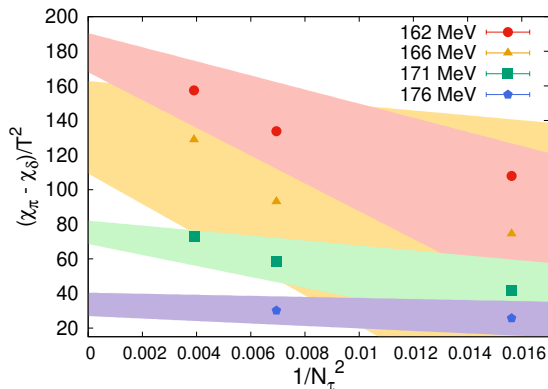


Fig. 4: The continuum estimates for $\chi_\pi - \chi_\delta$ normalized by the square of temperature for HISQ fermions from 3 different lattice spacings corresponding to $N_\tau = 8, 12, 16$ at $T = 162, 166, 171$ MeV respectively and from $N_\tau = 12, 16$ data at $T = 176$ MeV.

In the chiral symmetry restored phase, $\chi_\sigma = \chi_\pi$ and $\chi_\delta = \chi_\eta$ hence one obtains $\chi_\pi - \chi_\delta = 4\chi_{5\text{disc}}$. Using

chiral Ward identities it is known that $\chi_{5\text{disc}} = \chi_t/m^2$ where χ_t is the topological susceptibility of QCD. This allows relating the $U_A(1)$ breaking parameter to the topological susceptibility through the relation, $1/4(\chi_\pi - \chi_\delta)m_t^2/T^4 = \chi_t/T^4$. A comparison of these two observables is shown in Fig. 5. From the figure it is evident that for $T > 1.05 T_c$, when chiral symmetry is effectively restored, the two quantities agree with each other within errors. This is particularly interesting since for staggered quarks, even though the chiral and taste symmetries are intermixed at finite lattice spacing, the symmetries of QCD and related chiral Ward identities are recovered in the continuum limit.

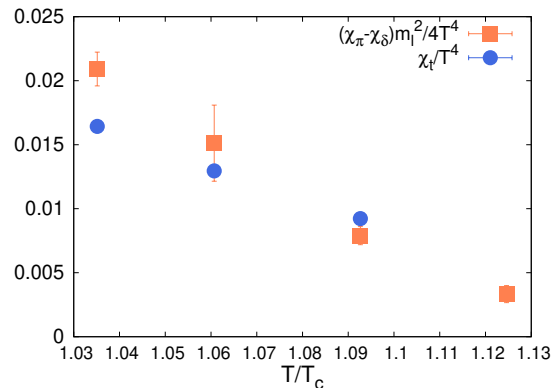


Fig. 5: A comparison of the integrated renormalized correlator $(\chi_\pi - \chi_\delta)m_t^2/4T^4$ with the topological susceptibility (measured independently using gradient flow in Ref. [50]) for temperatures $> T_c$.

Distribution of the smallest eigenvalue at finite temperature

The probability distribution of the smallest eigenvalue of the QCD Dirac operator λ_{\min} has inherent information about the microscopic degrees of freedom. For a random matrix ensemble (at zero temperature) the smallest eigenvalue is distributed according to,

$$P(c\lambda_{\min}) = \sqrt{\frac{\pi}{2}}(c\lambda_{\min})^{3/2}I_{3/2}(c\lambda_{\min})e^{-\frac{1}{2}(c\lambda_{\min})^2}, \quad (4)$$

At the lowest temperature $T = 145$ MeV, we calculate the probability distribution of the smallest eigenvalue λ_{\min} at different lattice spacings and perform a continuum estimate of the distributions, details of which are given in Appendix B. The final outcome of the fit is given in Fig. 6. The continuum extrapolation of the distribution shown as the orange band agrees well with the distribution of a chiral Gaussian unitary random matrix ensemble. In contrast, we also plot the distribution of the lowest eigenvalue at $T = 171$ MeV whose continuum extrapolation is shown as a blue band in Fig. 6. It is evident that the lowest eigenvalue which is a part of the near-zero peak follows a very different statistics rather than known from a chiral RMT.

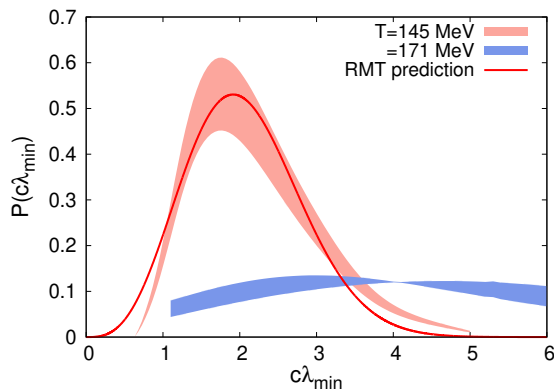


Fig. 6: The continuum extrapolated probability distribution of smallest eigenvalue for $T = 145, 171$ MeV shown as orange and blue bands respectively and its comparison with the RMT prediction.

Why is $U_A(1)$ effectively restored at temperature above T_c ? The next question we ask is whether the near-zero modes which arise due to interactions among instantons can distinctly disentangle out of the bulk modes. A similar phenomena occurs in disordered semi-metals leading to an Anderson-like transition. In such systems, with increasing strength of the disorder potential, there is a dynamical transition from a phase of delocalized electron states to that of localized states, with a certain energy threshold i.e., the *mobility edge* separating them. It is also known that near such an Anderson-like transition, the eigenvalue spacing distribution of the disordered states follows a similar behavior as RMTs for all spacing values except at the tails of the distribution due to the effects of the localized states. We observe the same features for the QCD Dirac eigen spacing distribution for our finest $N_\tau = 16$ lattices, detailed in Appendix C. In addition we have performed a systematic measurement of level-spacing distributions at different temperatures above T_c for different lattice spacings and extracted the parameters that characterize its functional dependence in the same Appendix. We find that the bulk modes (except at its higher tails) agree very well with the results obtained for random matrices belonging to Gaussian Unitary ensemble (GUE). Having shown the distinct features of near-zero and bulk modes, we have elaborated on how reliably we can estimate the temperature at which these modes separate in Appendix D. We obtain the temperature of $\sim 1.15(3) T_c$, which is similar to a *mobility edge* that separates the near-zero from the bulk modes.

In order to interpret these results, one could visualize the quarks moving in the background of an interacting ensemble of instantons, where the strength of the interactions changes as a function of temperature. At the microscopic level it is conjectured that the instantons remain strongly correlated below T_c , subsequently transitioning to a liquid-like phase with a finite correlation

length [51] just above T_c , and eventually to a gas-like phase at $2 T_c$ [13, 15]. Below T_c the intercept of the infrared eigenvalue density quantifies the chiral condensate which corresponds to the breaking of the non-singlet part of the chiral symmetry. Due to very strong correlations the microscopic details of the interactions are lost and the eigenvalues repel strongly similar to random matrices of a GU ensemble. As the temperature is increased, the interactions weaken and indeed at ~ 171 MeV, the near-zero eigenvalues with an oscillating behavior, as predicted from instanton liquid model, start to become prominent. These eventually separate from the bulk at $\sim 1.15 T_c$ analogous to opening of a mobility edge. Earlier studies have observed screening of inter-instanton interactions and build-up of local pockets of Polyakov loop fluctuations [38, 52] above such temperatures. This is also the region where the constituent dyons of the closely-spaced instantons interact semi-classically and thus start to become detectable [53–56].

Incidentally this suppression of long range instanton interactions also weakens the strength of $U_A(1)$ breaking, allowing for its *effective* restoration at $T \lesssim 1.15 T_c$. Lattice studies [57, 58] have reported a jump in the electrical conductivity around this temperature. This also suggests that the strength of the attractive potential due to instantons changes from liquid-like correlations to sparse local hot-spots, leaving most of the quark momentum states beyond the mobility edge to be delocalized thus enhancing the electrical charge transport.

Conclusions In this letter we have addressed a long-standing question of whether the flavor singlet $U_A(1)$ subgroup of the chiral symmetry gets effectively restored simultaneously with the non-singlet part for QCD with two light quark flavors at T_c . The effective restoration of the anomalous $U_A(1)$ symmetry is a non-perturbative phenomenon driven by the deep infra-red part of the QCD Dirac eigenvalue spectrum. By carefully performing the continuum extrapolation of the staggered Dirac spectrum on the lattice and studying in detail its properties, we explicitly demonstrate that $U_A(1)$ remains effectively broken in the chirally symmetric phase for $T \lesssim 1.15 T_c$. We also provide arguments for why this conclusion should remain unchanged even in the chiral limit.

With the increase in temperature the strength of interactions between the instantons starts weakening due to which the deep infrared part of the spectrum is separated out of the bulk modes which happens to be around $T \sim 1.15 T_c$. The tunneling probability due to instantons also decreases with increasing temperature which results in lowering of the height of near-zero peak of eigenvalue density. We show for the first time that both these phenomena are possibly the reason behind the $U_A(1)$ restoration, which also surprisingly happens to be around the same temperature. Observations of such rich interplay of phenomena in QCD matter above T_c should be quite robust, since these are made after performing a continuum extrapolation. It will be interesting to observe further finer details of chiral transition in the massless limit with

QCD Dirac operators which have exact chiral symmetry on the lattice.

Acknowledgements The authors acknowledge support by the Deutsche Forschungsgemeinschaft (DFG, German Research Foundation) through the CRC-TR 211 ‘Strong-interaction matter under extreme conditions’-Project no. 315477589 – TRR 211. S.S. acknowledges support by the Department of Science and Technology, Govt. of India through a Ramanujan Fellowship. The numerical computations in this work were performed on the GPU cluster at Bielefeld University. We thank the Bielefeld HPC.NRW team for their support. We thank the HotQCD Collaboration, specially Christian Schmidt for sharing the gauge configurations and software with us. We also acknowledge the contribution of Hiroshi Ohno who was involved during the early stages of the project. S.S. is grateful to Frithjof Karsch for helpful discussions and his kind hospitality when this work was finalized. A part of this work is based on the MILC collaboration’s public lattice gauge theory code [59].

Appendix A: Details of the lattice calculations of the eigenvalue spectrum

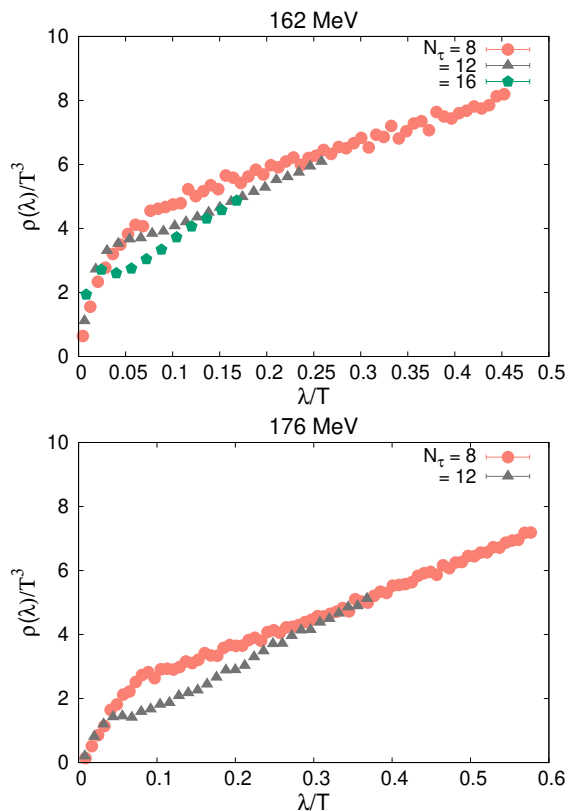


Fig. 7: The eigenvalue spectrum for HISQ Dirac operator at three different lattice spacings corresponding to $N_\tau = 8, 12, 16$ for $T = 162$ MeV and at $N_\tau = 8, 12$ for $T = 176$ MeV.

We first tabulate the lattice sizes, gauge couplings and the number of configurations that we have studied for each temperature value from 145-176 MeV in Table I. As

mentioned earlier, it is important that we take the continuum limit appropriately hence for each temperature we performed calculations with three different lattice extents $N_\tau = 8, 12, 16$ in order to perform continuum extrapolation of the parameters characterizing the eigenvalue density. We then calculated the first 60, 100, 200 eigenvalues of the massless HISQ Dirac matrix for $N_\tau = 16, 12, 8$ respectively. We have fixed the bin size $\lambda a = 0.001$ for each N_τ for measuring the eigenvalue density and performed a jack-knife analysis to remove any auto-correlation effects among the data in the bins. We then fit the bulk part i.e. all eigenvalues above an infrared cut-off $\lambda > \lambda_0$ with the fit ansatz $\frac{\rho(\lambda)}{T^3} = \frac{\lambda}{T} \cdot \frac{c_1(T, m)}{T^2} + \frac{\rho_0}{T^3}$. The results of the fit and the choice of cut-off at different temperatures are mentioned in Table II.

T (MeV)	β	N_s	N_τ	N_{conf_s}
145	6.285	48	12	1530
145	7.010	64	16	2860
162	6.423	32	8	250
162	6.825	48	12	1960
162	7.130	64	16	3390
166	6.445	32	8	400
166	6.850	48	12	2100
166	7.156	64	16	2190
171	6.474	32	8	280
171	6.880	48	12	1980
171	7.188	64	16	1040
176	6.500	32	8	240
176	6.910	48	12	330

Tab. I: The parameters for the lattice calculations

T [MeV]	N_τ	λ_0/T	$\frac{c_1}{T^2}$	ρ_0/T^3
145	12	0.1	9.0(5)	7.30(7)
145	16	0.05	9(1)	6.67(9)
162	8	0.2	8.8(3)	4.1(1)
162	12	0.15	13.2(2)	2.69(5)
162	16	0.1	17.5(5)	1.93(7)
166	8	0.2	8.9(1)	3.31(5)
166	12	0.15	13.3(3)	1.92(6)
166	16	0.1	16.6(8)	1.4(1)
171	8	0.2	9.3(1)	2.38(5)
171	12	0.15	12.9(1)	1.19(3)
171	16	0.1	17.0(5)	0.45(8)
176	8	0.2	9.5(1)	1.67(4)
176	12	0.15	13.0(2)	0.36(6)

Tab. II: Lattice size ($N_\sigma^3 \times N_\tau$), temperature (T), the estimated values of c_1/T^2 and ρ_0/T^3 after the fit of the bulk modes by taking the lower cutoff at λ_0/T .

We have shown the eigenvalue distributions for three different temperatures at 145, 166, 171 MeV in Fig. 1. We also have measured the eigenvalue densities at two other temperatures at 166, 176 MeV which we show in Fig. 7.

Appendix B: Details of the calculation performed for the smallest eigenvalues for $T < T_c$

First we have extracted the smallest eigenvalue from each configuration for $N_\tau = 12, 16$ and later re-scaled to the dimensionless quantity $c\lambda_{\min}$, where the value of $\langle \bar{\psi}\psi \rangle$ at finite temperature is obtained from Ref. [60]. Keeping the bin size constant we obtained the probability distribution of $c\lambda_{\min}$ for each N_τ and then performed a spline interpolation by taking appropriate weights proportional to the errors for each data point in order to have a smoother interpolating curve. Next we performed a continuum extrapolation at each value of $c\lambda_{\min}$ of the interpolating function with the ansatz $c + d/N_\tau^2$. We assigned a 15% error for $T = 145$ MeV, as we only had two points while performing the continuum extrapolation. In Fig. 6 we find a good agreement between the continuum extrapolated distribution of the lowest eigenvalue at $T = 145$ MeV and the RMT predictions from a Gaussian Unitary ensemble. A slight discrepancy exist for lower and higher values of $c\lambda_{\min}$. This can be due to the fact that we use a very low but finite convergence criterion while calculating the eigenvalue spectrum. Hence we do not have any data for $c\lambda_{\min} < 0.6$. Since we are plotting a probability distribution (of the smallest eigenvalue), the area under the curve must be unity. To preserve this criterion the values of the probability densities along the higher end of the tail lie above the RMT curve in order to compensate for the relatively lower values in the lower portion of the tail.

Appendix C: The level spacing distribution for bulk modes

Next we look at the level spacing distribution of the bulk modes. To study the universal properties of the eigenvalue level spacing fluctuations one has to remove the system dependent mean. This is done by a method called unfolding. Let λ represent eigenvalues in the ascending sequence for any particular gauge configuration. The average density of the eigenvalues in the sequence i.e. the reciprocal of the average spacing as a function of λ is represented as $\bar{\rho}(\lambda)$. The eigenvalue sequence can then be unfolded using the average level-staircase function, $\bar{\eta}(\lambda) = \int_{\lambda_0}^{\lambda} d\lambda' \bar{\rho}(\lambda')$ which tells us how many eigenvalues in this sequence are less than λ on an average. Here λ_0 labels the eigenvalue beyond which all the higher eigenvalues are bulk modes and below which are the near-zero modes. The unfolded sequence is labeled by $\lambda_i^{uf} = \bar{\eta}(\lambda_i)$, where the index i labels the original eigenvalue whose unfolding is performed. When appropriately normalized, the average spacing between the unfolded eigenvalues equals unity. The nearest neighbor spacing distribution is constructed by calculating the differences between consecutive unfolded eigenvalues $\lambda_{i+1}^{uf} - \lambda_i^{uf}$ and organizing them into histogram bins. This gives us a picture of how the eigenvalue spacings fluctuate about the average which

we have plotted in Fig. 8 for four different temperatures $T = 162, 166, 171, 176$ MeV and at each temperature, for the three different lattice sizes $N_\tau = 8, 12, 16$ except for $T = 176$ MeV. We have then estimated the functional dependence of these nearest neighbor spacing distributions by two different fit ansatz, shown as solid and dotted lines in Fig. 8. The dotted curves were obtained after performing a fit to the lattice data points with the function $f(s) = as^b e^{-cs^2}$, motivated by the Wigner surmise. The solid curves on the other hand, were obtained after fitting the points to an ansatz function $f(s) = ps^2 e^{-qs^2}$. The values of these parameters a, b, c, p, q after performing the fits are given in Table III. It is evident that the level repulsion between the bulk modes is quadratic similar to that of random matrices belonging to the Gaussian unitary ensemble (GuE). However for the $N_\tau = 16$ lattices, due to the contamination with the near-zero modes the fit of the tail is not good and can not be explained by RMT prediction. In order to account for the long tail of the spacing distribution we fit it to a semi-Poisson distribution $P(s) \sim s^2 \exp(-\alpha s)$ which shows strong repulsion at small values of s but falls off slowly at large values of s parameterized by a fit parameter α . After performing the fit of the level separation with this ansatz, we obtain the value of $\alpha = 3.02(7), 3.17(9), 3.3(1)$ for temperatures $T = 162, 166, 171$ MeV respectively. The lattice data now do agree to this new fit ansatz reasonably well for $N_\tau = 16$ at all temperatures above T_c , which is evident in Fig. 9.

T (MeV)	N_τ	a	b	c	p	q
162	8	2.91(5)	1.85(3)	1.19(1)	3.16(7)	1.26(2)
162	12	2.6(1)	1.69(6)	1.13(3)	3.2(1)	1.29(3)
162	16	2.1(4)	1.2(2)	1.0(1)	4.0(6)	1.6(1)
166	8	2.78(5)	1.78(2)	1.16(1)	3.13(9)	1.26(2)
166	12	2.6(2)	1.66(7)	1.12(4)	3.2(2)	1.30(4)
166	16	2.1(5)	1.2(2)	1.1(2)	4.5(8)	1.8(2)
171	8	2.74(7)	1.76(3)	1.15(2)	3.2(1)	1.27(2)
171	12	2.5(2)	1.6(1)	1.11(6)	3.4(3)	1.35(6)
171	16	1.6(4)	0.8(2)	1.0(2)	5(1)	2.0(3)
176	8	2.77(7)	1.77(4)	1.16(2)	3.15(9)	1.27(2)
176	12	2.3(3)	1.4(1)	1.07(8)	3.5(3)	1.39(7)

Tab. III: The estimated values of the parameters after the fit to different unfolded level spacing distributions.

Appendix D: Details of extraction of the mobility edge

Next, in order to estimate when these bulk modes separate from the deep-infrared peak of eigenvalues, we calculate at what temperature the functional fit of the bulk eigenvalue spectrum has a non-zero intercept along the λ -axis which is larger than the typical width of the near-zero peak. In the continuum, we have already calculated the slope of the bulk eigenvalue density, which is $c_1(m, T)/T^2 = 16.8(4)$. Looking at the eigenvalue distributions in Fig.1, we can choose a typical value of λ at

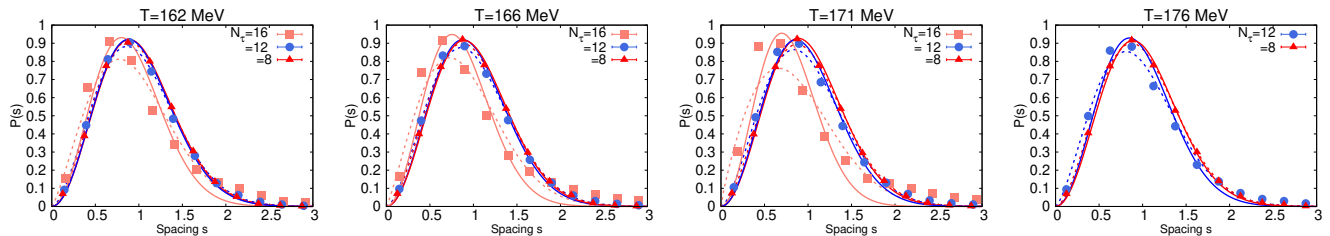


Fig. 8: Unfolded level spacing distribution of bulk eigenvalues modes for different temperatures shown as a function of different lattice spacings or equivalently, N_τ . The solid lines in each plot correspond to the two-parameter fit and the dotted curves for three-parameter fits inspired from the Wigner surmise for Gaussian unitary random matrix ensembles.

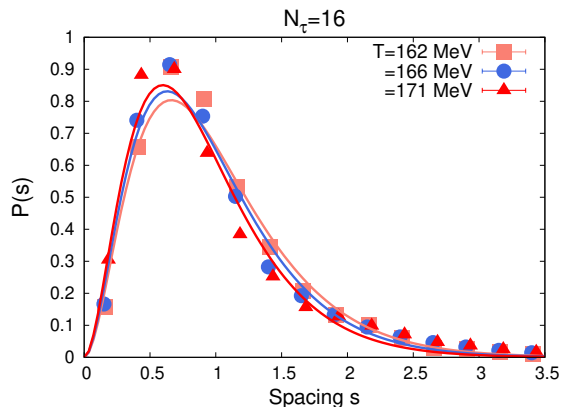


Fig. 9: A fit to the eigenvalue level spacing distribution using a mixed ansatz for $N_\tau = 16$ at $T = 162, 166, 171$ MeV.

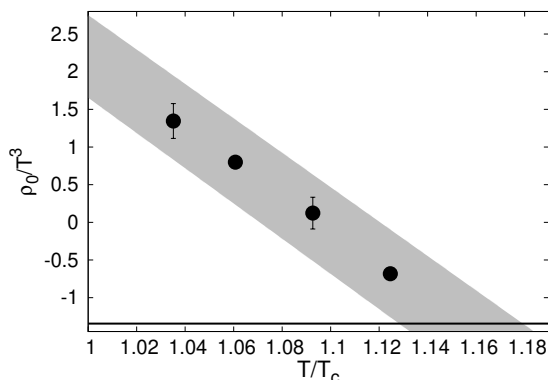


Fig. 10: Continuum extrapolation of the bulk intercept for eigenvalue densities at different temperatures above T_c . The horizontal line corresponds to $\rho_0/T^3 = -1.34$ for the bulk spectrum when it is completely separates from near zero modes.

which the near-zero and bulk modes separate out, which is most evident for the $N_\tau = 16$ lattices at $\lambda_0/T \sim 0.08$. Using these inputs and that the bulk modes have a linear-in- λ dependence we can calculate the value of bulk intercept $\rho_0/T^3 = -1.34$ at $\lambda = 0$. Next we take the values of the intercept of bulk mode density for all $T > T_c$ from Table II and perform a continuum extrapolation with the function $\rho_0/T^3 + d/N_\tau^2$. The continuum values, ρ_0/T^3 so-obtained are shown in Fig. 10 for all $T > T_c$. At the highest temperature $T = 176$ MeV a 10% error is assigned to the data point since we could perform a continuum estimate with the data available only for two N_τ values. Now fitting the continuum extrapolated values, ρ_0/T^3 with the ansatz $\rho_0/T^3 = d_1(T/T_c) + d_2$ we obtain $d_1 = -23.1(3)$ and $d_2 = 25.3(3)$. Using this parametric dependence of the continuum value of the intercept as a function of temperature, we extract a $T/T_c = 1.15(3)$ when the value of $\rho_0/T^3 = -1.34$ i.e., when the near-zero modes distinctly emerge out from the bulk spectrum.

[1] T. Banks and A. Casher, Nucl. Phys. B **169**, 103 (1980).
 [2] H. Leutwyler and A. V. Smilga, Phys. Rev. D **46**, 5607 (1992).

[3] A. Bazavov et al. (HotQCD), Phys. Lett. B **795**, 15 (2019), 1812.08235.

[4] R. D. Pisarski and F. Wilczek, Phys. Rev. D **29**, 338

- (1984).
- [5] A. Butti, A. Pelissetto, and E. Vicari, *JHEP* **08**, 029 (2003), hep-ph/0307036.
- [6] A. Pelissetto and E. Vicari, *Phys. Rev. D* **88**, 105018 (2013), 1309.5446.
- [7] S. Sharma (HotQCD), *PoS CPOD2017*, 086 (2018).
- [8] M. P. Lombardo and A. Trunin, *Int. J. Mod. Phys. A* **35**, 2030010 (2020), 2005.06547.
- [9] A. Bazavov et al. (HotQCD), *Phys. Rev. D* **86**, 094503 (2012), 1205.3535.
- [10] M. I. Buchoff et al., *Phys. Rev. D* **89**, 054514 (2014), 1309.4149.
- [11] T. Bhattacharya et al., *Phys. Rev. Lett.* **113**, 082001 (2014), 1402.5175.
- [12] V. Dick, F. Karsch, E. Laermann, S. Mukherjee, and S. Sharma, *Phys. Rev. D* **91**, 094504 (2015), 1502.06190.
- [13] P. Petreczky, H.-P. Schadler, and S. Sharma, *Phys. Lett. B* **762**, 498 (2016), 1606.03145.
- [14] A. Bazavov et al., *Phys. Rev. D* **100**, 094510 (2019), 1908.09552.
- [15] H. T. Ding, S. T. Li, S. Mukherjee, A. Tomiya, X. D. Wang, and Y. Zhang, *Phys. Rev. Lett.* **126**, 082001 (2021), 2010.14836.
- [16] O. Kaczmarek, L. Mazur, and S. Sharma, *Phys. Rev. D* **104**, 094518 (2021), 2102.06136.
- [17] G. Cossu, S. Aoki, H. Fukaya, S. Hashimoto, T. Kaneko, H. Matsufuru, and J.-I. Noaki, *Phys. Rev. D* **87**, 114514 (2013), [Erratum: *Phys.Rev.D* 88, 019901 (2013)], 1304.6145.
- [18] T.-W. Chiu, W.-P. Chen, Y.-C. Chen, H.-Y. Chou, and T.-H. Hsieh (TWQCD), *PoS LATTICE2013*, 165 (2014), 1311.6220.
- [19] A. Tomiya, G. Cossu, S. Aoki, H. Fukaya, S. Hashimoto, T. Kaneko, and J. Noaki, *Phys. Rev. D* **96**, 034509 (2017), [Addendum: *Phys.Rev.D* 96, 079902 (2017)], 1612.01908.
- [20] B. B. Brandt, A. Francis, H. B. Meyer, O. Philipsen, D. Robaina, and H. Wittig, *JHEP* **12**, 158 (2016), 1608.06882.
- [21] S. Aoki, Y. Aoki, G. Cossu, H. Fukaya, S. Hashimoto, T. Kaneko, C. Rohrhofer, and K. Suzuki (JLQCD), *Phys. Rev. D* **103**, 074506 (2021), 2011.01499.
- [22] S. Aoki, Y. Aoki, H. Fukaya, S. Hashimoto, C. Rohrhofer, and K. Suzuki (JLQCD), *PTEP* **2022**, 023B05 (2022), 2103.05954.
- [23] E. V. Shuryak and J. J. M. Verbaarschot, *Nucl. Phys. A* **560**, 306 (1993), hep-th/9212088.
- [24] J. J. M. Verbaarschot and I. Zahed, *Phys. Rev. Lett.* **70**, 3852 (1993), hep-th/9303012.
- [25] J. J. M. Verbaarschot, *Phys. Rev. Lett.* **72**, 2531 (1994), hep-th/9401059.
- [26] M. E. Berbenni-Bitsch, S. Meyer, A. Schafer, J. J. M. Verbaarschot, and T. Wettig, *Phys. Rev. Lett.* **80**, 1146 (1998), hep-lat/9704018.
- [27] G. Akemann, P. H. Damgaard, U. Magnea, and S. Nishigaki, *Nucl. Phys. B* **487**, 721 (1997), hep-th/9609174.
- [28] A. D. Jackson, M. K. Sener, and J. J. M. Verbaarschot, *Nucl. Phys. B* **506**, 612 (1997), hep-th/9704056.
- [29] A. M. Garcia-Garcia and J. J. M. Verbaarschot, *Nucl. Phys. B* **586**, 668 (2000), hep-th/0003159.
- [30] G. Akemann and T. R. Würfel, *JHEP* **12**, 128 (2021), 2110.03617.
- [31] M. Giordano and T. G. Kovacs, *Universe* **7**, 194 (2021), 2104.14388.
- [32] J. J. M. Verbaarschot, *Nucl. Phys. B* **427**, 534 (1994), hep-lat/9402006.
- [33] A. M. Garcia-Garcia and J. C. Osborn, *Phys. Rev. D* **75**, 034503 (2007), hep-lat/0611019.
- [34] T. G. Kovacs and F. Pittler, *Phys. Rev. Lett.* **105**, 192001 (2010), 1006.1205.
- [35] T. G. Kovacs and F. Pittler, *Phys. Rev. D* **86**, 114515 (2012), 1208.3475.
- [36] M. Giordano, T. G. Kovacs, and F. Pittler, *Phys. Rev. Lett.* **112**, 102002 (2014), 1312.1179.
- [37] M. Giordano, S. D. Katz, T. G. Kovacs, and F. Pittler, *JHEP* **02**, 055 (2017), 1611.03284.
- [38] L. Holicki, E.-M. Ilgenfritz, and L. von Smekal, *PoS LATTICE2018*, 180 (2018), 1810.01130.
- [39] T. G. Kovacs and R. A. Vig, *Phys. Rev. D* **97**, 014502 (2018), 1706.03562.
- [40] P. W. Anderson, *Phys. Rev.* **109**, 1492 (1958).
- [41] A. Alexandru and I. Horváth, *Phys. Lett. B* **833**, 137370 (2022), 2110.04833.
- [42] A. Alexandru and I. Horváth, *Phys. Rev. D* **100**, 094507 (2019), 1906.08047.
- [43] A. Alexandru and I. Horváth, *Phys. Rev. Lett.* **127**, 052303 (2021), 2103.05607.
- [44] A. Bazavov et al., *Phys. Rev. D* **95**, 054504 (2017), 1701.04325.
- [45] A. V. Smilga and J. Stern, *Phys. Lett. B* **318**, 531 (1993).
- [46] S. Aoki, H. Fukaya, and Y. Taniguchi, *Phys. Rev. D* **86**, 114512 (2012), 1209.2061.
- [47] J. J. M. Verbaarschot, *Nucl. Phys. B Proc. Suppl.* **53**, 88 (1997), hep-lat/9607086.
- [48] Y. Aoki et al. (Flavour Lattice Averaging Group (FLAG)), *Eur. Phys. J. C* **82**, 869 (2022), 2111.09849.
- [49] E. V. Shuryak, *Comments Nucl. Part. Phys.* **21**, 235 (1994), hep-ph/9310253.
- [50] L. Mazur, Ph.D. thesis, Bielefeld U. (2021).
- [51] T. Schäfer and E. V. Shuryak, *Rev. Mod. Phys.* **70**, 323 (1998), hep-ph/9610451.
- [52] F. Bruckmann, T. G. Kovacs, and S. Schierenberg, *Phys. Rev. D* **84**, 034505 (2011), 1105.5336.
- [53] V. G. Bornyakov, E. M. Ilgenfritz, B. V. Martemyanov, and M. Müller-Preussker, *Phys. Rev. D* **93**, 074508 (2016), 1512.03217.
- [54] R. N. Larsen, S. Sharma, and E. Shuryak, *Phys. Lett. B* **794**, 14 (2019), 1811.07914.
- [55] R. N. Larsen, S. Sharma, and E. Shuryak, *Phys. Rev. D* **102**, 034501 (2020), 1912.09141.
- [56] R. N. Larsen, S. Sharma, and E. Shuryak, *Phys. Rev. D* **105**, L071501 (2022), 2112.04537.
- [57] A. Amato, G. Aarts, C. Allton, P. Giudice, S. Hands, and J.-I. Skullerud, *Phys. Rev. Lett.* **111**, 172001 (2013), 1307.6763.
- [58] G. Aarts, C. Allton, A. Amato, P. Giudice, S. Hands, and J.-I. Skullerud, *JHEP* **02**, 186 (2015), 1412.6411.
- [59] <http://physics.utah.edu/~detar/milc.html>.
- [60] P. Steinbrecher, Ph.D. thesis, U. Bielefeld (main) (2018).